An Empirical Model for Specularity Prediction with Application to Dynamic Retexturing

Alexandre Morgand*
CEA, LIST, Vision & Content Engineering Lab / ISIT

Mohamed Tamaazousti †
CEA, LIST, Vision & Content Engineering Lab

Adrien Bartoli‡
ISIT

Abstract

Specularities, which are often visible in images, may be problematic in computer vision since they depend on parameters which are difficult to estimate in practice. We present an empirical model called JOLIMAS: JOint LIght-MAterial Specularity, which allows specularity prediction. JOLIMAS is reconstructed from images of specular reflections observed on a planar surface and implicitly includes light and material properties which are intrinsic to specularities. This work was motivated by the observation that specularities have a conic shape on planar surfaces. A theoretical study on the well known illumination models of Phong and Blinn-Phong was conducted to support the accuracy of this hypothesis. A conic shape is obtained by projecting a quadric on a planar surface. We showed empirically the existence of a fixed quadric whose perspective projection fits the conic shaped specularity in the associated image. JOLIMAS predicts the complex phenomenon of specularity using a simple geometric approach with static parameters on the object material and on the light source shape. It is adapted to indoor light sources such as light bulbs or fluorescent lamps. The performance of the prediction was convincing on synthetic and real sequences. Additionally, we used the specularity prediction for dynamic retexturing and obtained convincing rendering results. Further results are presented as supplementary material.

1 Introduction

The photometric phenomenon of specular reflections is often seen in images. Specularities occur on surfaces when their imperfections are smaller than the incident wavelength making them mirror-like. In that case, light is completely reflected in a specular form (the angles of reflection and incidence are equal w.r.t the normal of the surface) creating a specular highlight in the image. Specularities are important in several fields. They often saturate the camera response and may impact the rest of the image. This abrupt change of the image intensity disturbs computer vision algorithms such as camera localization, tracking or 3D reconstruction. However, instead of treating these specularities as perturbations or outliers, they may be considered as useful primitives. In fact, specularities give additional information about the depth of the scene [10, 31] and may improve camera localization [21, 24, 34], 3D reconstruction [10, 32] and scene material analysis [5, 26, 27, 33]. In Augmented Reality (AR) and computer graphics, these primitives allow significant improvement of rendering quality [8, 11, 12, 16, 17, 19, 30, 31]. Indeed, it was showed that specularities play a key role in scene perception by the human brain [1]. To achieve better results for these applications, specularity prediction for a given viewpoint and a scene is tremendously important.

By observing the shape of a specularity on a planar surface, it seems plausible to model it by a conic. The latter is obtained by projecting a quadric on a plane. Considering these elements, it is natural to ask if it would be possible to reconstruct a fixed quadric explaining the specularity for every viewpoint. If possible, this model would represent a link between the photometric phenomenon of specularities (light and material) and multiple view geometry [14]. We propose JOLIMAS, an empirical model which allows us to easily predict the position and shape of specularities from existing and new viewpoints, as illustrated in figure 1. This model is composed of a quadric which implicitly captures light and material properties, which are intrinsic to specularities. This quadric is reconstructed from the conics associated with the specularity. We work essentially on planar surfaces because they are dominant in the indoor context [4, 16]. With JOLIMAS, we collect experimental evidence to answer the above mentioned modeling hypothesis: it turns out that the shape of specularities can be very well approximated by a purely quadric based model. We work essentially with specularities clearly visible (high intensity) because their impact on computer vision algorithms is too high as opposed to smooth specularities. When planar surfaces of strong roughness affects the specularity contours, our conic approximation is still relevant because our model is abstracting this parameter along with the reflectance of the surface material.

JOLIMAS is presented in section 3. Its estimation is detailed in section 4 by comparing the different state of the art approaches for quadric reconstruction. This empirical model, along with the specularity predictions, is tested on synthetic and real sequences including bulb and fluorescent lamps in section 5. We present an application to specularity prediction on real sequences for retexturing in section 6.

(a)

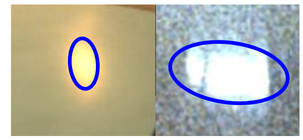

(b)

(c)

(d)

Figure 1: We observe that specularities have a conic shape on planar surfaces. We approximate them by projecting a fixed quadric which includes light and material properties. This figure presents quadric reconstruction examples (blue quadrics) for two light types (light bulb (c) and fluorescent lamp (d)) and two materials (steel table (c) and a plastic kitchen counter (d)). The lights sources along with the steel table and the plastic kitchen counter can be seen in (a). Once reconstructed, our virtual quadric model allows the prediction of future specular reflections by simple perspective projection (blue conics). (b) shows the specularity prediction close-up in the respective sequences.

*e-mail:alexandre.morgand@cea.fr
†e-mail:mohamed.tamaazousti@cea.fr
‡e-mail:adrien.bartoli@gmail.com

2 State of the Art

Specularity prediction is a difficult problem because a specularity is a complex photometric phenomenon described by its size, position, shape and intensity. Additionally, these elements are highly influenced by the camera (its pose and response function), the scene including its geometry and material (reflectance and roughness) and the light sources (position, shape, intensity, isotropicity). There is currently no methods to estimate a predictive specularity model from images. A natural approach would be to estimate a physical model of the scene with the associated parameters for the materials and light sources. As opposed to camera localization and 3D scene geometric reconstruction, the estimation of these parameters is possible but extremely difficult and ill-posed in practice when only an image sequence is available. Existing methods estimate the light sources. They can be divided in two categories: global illumination and primary source reconstruction.

For global illumination, Jacknik *et al.* [16] proposed light environment map reconstruction from a video of a planar specular surface. This method uses a GPU implementation and achieves a convincing photo-realistic rendering for AR application. However, this model does not distinguish primary and secondary sources, which is essential for specularity prediction for unknown viewpoints. Meilland *et al.* [23] also present a global illumination estimation by reconstructing primary sources as point lights. They are directly observed from an RGB-D camera. Despite its high quality rendering, the method lacks flexibility. In fact, the method represents a volumetric light source such as fluorescent light by a set of point lights. Therefore, the method has to compute an intensity for each of the different points which are supposed to represent the same light. Moreover, dynamical light sources (lights changing intensity over time) are not handled and specular materials are not modeled. As a consequence, this method cannot predict specular reflections for new viewpoints.

Solutions have been also proposed to the primary light source reconstruction problem. Ideally, every physical light model has to be associated with a geometry (position and shape), color [22] and intensity value to realistically match the lighting conditions of the scene. Even though many light models exist in computer graphics, the ones used for light source reconstruction in computer vision are generally divided in two categories: directional light sources and point light sources. Lagger *et al.* [20] describe a method to compute directional lights using specular reflections on a mobile object observed from a fixed viewpoint. This application is limited as due to the view-dependent aspect of specular reflections, light sources should be estimated for each position. Neither shape, position nor object material are taken into account, making the method unable to predict specular reflections. Similar approaches [4, 18, 38] experience the same issues with the same limitations. On point light source estimation, Boom *et al.* approach [3] computes a primary light source assuming Lambertian surfaces and using an RGB-D camera. From the diffuse term, by comparing synthesis rendering with the real scene, a point light is estimated. However, this method is not suitable for real-time applications and for volumetric light estimation as fluorescent lamps. By computing only one light source without its shape and the associated specular material properties, specularity prediction can not be achieved.

To predict a specularity from physical light source reconstruction, complex parameters of light and materials have to be computed. In practice, a physical approach as the ones described previously does not seem practical, as we only have an image sequence and camera pose as inputs. To address this challenging highly non-linear problem, we propose a quadric based model reconstructed from conics fitted to specularities on each viewpoint. Despite its simplicity, this empirical model, implicitly capturing the light source and material parameters, allows specularity prediction in new viewpoints.

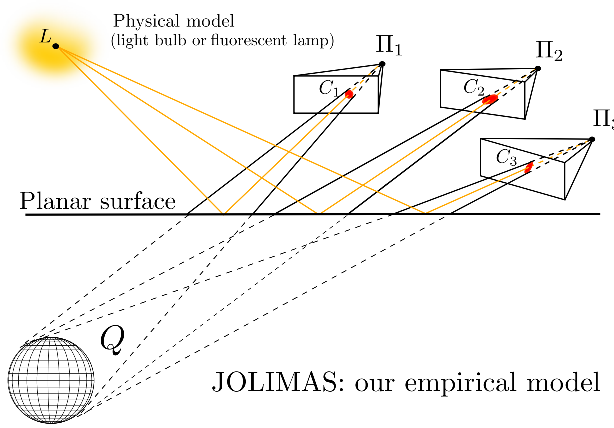

Figure 2: JOLIMAS illustration, showing the link between photometry (light and surface material) and multiple view geometry (our empirical model). The light source L which could be either a light bulb or a fluorescent lamp is creating specularities (the red conics) in the different viewpoints Π_1, Π_2 and Π_3. From multiple viewpoints, a quadric Q is reconstructed from specular reflections of conic shape in the images (C_1, C_2 and C_3). We then use the quadric Q projected onto the planar surface to predict specularities in new viewpoints.

3 Modeling

We propose JOLIMAS an empirical model, including light source and materials properties. JOLIMAS uses a quadric reconstructed from conics fitted to the specularity for each viewpoint as illustrated in figure 2. We assume a non-Lambertian planar surfaces where each specularity is associated with a light source. A formal demonstration of our conic specularity approximation on a planar surface is given in the following section. We then evaluate our elliptical specularity hypothesis on planar surfaces empirically.

3.1 Theoretical Motivation

Phong model. We choose the Phong illumination model [28] which is the baseline in most BRDF models [15]. This illumination model divides the image in three components: the diffuse, ambient and specular ones. Recent models such as Blinn-Phong [2], Ward [37], Cook-Torrance [6] differ in the way the specular term is computed. These models propose improved roughness computation. Even if the Phong specular term is no longer used in rendering, it perfectly suits the approximation in our study. Indeed, roughness is implicitly included in the proposed JOLIMAS model.

The Phong intensity function of a 3D surface point $\mathbf{p}$ is given by:

$$I(\mathbf{p}) = i_a k_a + i_d k_d (\hat{\mathbf{L}}(\mathbf{p}) \cdot \hat{\mathbf{N}}) + i_s k_s (\hat{\mathbf{R}}(\mathbf{p}) \cdot \hat{\mathbf{V}}(\mathbf{p}))^n, \tag{1}$$

with $\hat{\mathbf{R}}$ the normalized direction of a perfectly reflected ray of light $\hat{\mathbf{L}}$, $\hat{\mathbf{V}}$ the normalized direction pointing towards the viewer, n the glossiness of the surface, k_s, k_a and k_d the ratio of reflection of the specular, ambient and diffuse terms of incoming light, $\hat{\mathbf{N}}$ the normal of the surface S and i_s, i_a and i_d the incoming intensities on the surface for the specular, ambient and diffuse term. We choose the world coordinate frame so that the scene's flat surface $S \subset \mathbb{R}^3$ is the $(\mathbf{XY})$ plane. In other words, $S = \{\mathbf{P} \in \mathbb{R}^3 | P_Z = 0\}$. We can thus parameterize S by a point $\mathbf{p} \in \mathbb{R}^2$ and define $\mathbf{P} = \mathrm{stk}(\mathbf{p}, 0)$ with stk the stack operator for notation simplicity.

Specular term. At point $\mathbf{p}$, the specular component I_s is given by:

$$I_s(\mathbf{p}) = i_s k_s (\hat{\mathbf{R}}(\mathbf{p}) \cdot \hat{\mathbf{V}}(\mathbf{p}))^n, \tag{2}$$

We want to analyze the isocontours of a specular highlight on the surface S for a viewpoint $\mathbf{V}$, a light source $\mathbf{L}$ and $\mathbf{R} =$

$\mathrm{stk}(L_X, L_Y, -L_Z)$. We first expand equation (13) for a general τ and then solve it for $\tau = 1$ and $\tau = 0$.

$$I_s(\mathbf{p}) = \tau. \tag{3}$$

Because I_s is a scalar product between two normalized vectors, we have $-1 \leq I_s \leq 1$. Moreover, because $P_Z = 0$, $R_Z < 0$ and $V_Z > 0$, $I_s > 0$. Overall, $0 < I_s \leq 1$. By expanding the specular term of equation (16) and collecting the monomials of same degrees, we have:

$$\begin{aligned}
&(d^\circ 4)\ (1-\tau^2)||\mathbf{P}||^4 \\
&(d^\circ 3)\ 2(\tau^2-1)(\mathbf{R}+\mathbf{V})^\top \mathbf{P}||\mathbf{P}||^2 \\
&(d^\circ 2)\ \mathbf{P}^\top(\mathbf{R}\mathbf{R}^\top + 2\tau(1-2\tau^2)\mathbf{R}\mathbf{V}^\top + \\
&\qquad (2\mathbf{R}^\top\mathbf{V} - \tau^2||\mathbf{R}||^2 - \tau^2||\mathbf{V}||^2)\mathtt{I})\mathbf{P} \\
&(d^\circ 1)\ 2(-\mathbf{R}^\top\mathbf{V}\mathbf{R}^\top - \mathbf{R}^\top\mathbf{V}\mathbf{V}^\top + \\
&\qquad \tau^2||\mathbf{R}||^2\mathbf{V}^\top + \tau^2||\mathbf{V}||^2\mathbf{R}^\top)\mathbf{P} \\
&(d^\circ 0)\ (\mathbf{R}^\top\mathbf{V})^2 - \tau^2||\mathbf{R}||^2||\mathbf{V}||^2.
\end{aligned}$$

We observe that the sum of degrees 3 and 4 factors as:

$$(1-\tau^2)||\mathbf{P}||^2\mathbf{P}^\top(\mathbf{P} - 2\mathbf{R} - 2\mathbf{V}). \tag{4}$$

The brightest point. For the highest intensity value $\tau = 1$, monomials of degrees 3 and 4 vanish such as the remaining terms form a quadratic equation such as:

$$\tilde{\mathbf{P}}^\top \mathtt{Q} \tilde{\mathbf{P}} = 0, \tag{5}$$

where $\tilde{\mathbf{P}} \stackrel{\text{def}}{=} \mathrm{stk}(\mathbf{P}, 1)$ are the homogeneous coordinates of $\mathbf{P}$. Matrix $\mathtt{Q} \in \mathbb{R}^{4\times 4}$ is symmetric and defined by:

$$\mathtt{Q} = \begin{bmatrix} [\mathbf{R}-\mathbf{V}]_\times^2 & [\mathbf{V}\times\mathbf{R}]_\times(\mathbf{V}-\mathbf{R}) \\ ([\mathbf{V}\times\mathbf{R}]_\times(\mathbf{V}-\mathbf{R}))^\top & (\mathbf{R}^\top\mathbf{V})^2 - ||\mathbf{R}||^2||\mathbf{V}||^2 \end{bmatrix}$$

In the supplementary materials, we explain how $\mathrm{rank}(\mathtt{Q}) = 2$ and $\mathtt{Q}$ is non-negative meaning that $\mathtt{Q}$ is a point quadric representing the line containing $\mathbf{R}$ and $\mathbf{V}$. Its intersection with S is defined as the brightest point.

The outer contour. To further understand the structure of the problem, we solve it for the lowest intensity value $\tau = 0$ to study the nature of the outer contour. Expanding the specular term of equation (16), we obtain:

$$||\mathbf{P}||^2 - (\mathbf{R}+\mathbf{V})^\top\mathbf{P} + \mathbf{R}^\top\mathbf{V} = 0, \tag{6}$$

Which corresponds to a quadric surface and more particularly a sphere whose point matrix is:

$$\mathtt{Q} = \begin{bmatrix} \mathtt{I}_3 & -\frac{1}{2}(\mathbf{R}+\mathbf{V}) \\ -\frac{1}{2}(\mathbf{R}+\mathbf{V})^\top & \mathbf{R}^\top\mathbf{V} \end{bmatrix}. \tag{7}$$

By defining the orthographic projection on S as:

$$\mathtt{A} = \begin{bmatrix} 1 & 0 & 0 \\ 0 & 1 & 0 \\ 0 & 0 & 0 \\ 0 & 0 & 1 \end{bmatrix}, \tag{8}$$

the highlight's outer ring is thus given by the conic:

$$\mathtt{C} = \mathtt{A}^\top\mathtt{Q}\mathtt{A} = \begin{bmatrix} \mathtt{I}_2 & -\frac{1}{2}(\bar{\mathbf{R}}+\bar{\mathbf{V}}) \\ -\frac{1}{2}(\bar{\mathbf{R}}+\bar{\mathbf{V}})^\top & \mathbf{R}^\top\mathbf{V} \end{bmatrix},$$

with $\bar{\mathbf{R}} \stackrel{\text{def}}{=} \mathrm{stk}(\mathbf{R}_X, \mathbf{R}_Y)$ and $\bar{\mathbf{V}} \stackrel{\text{def}}{=} \mathrm{stk}(\mathbf{V}_X, \mathbf{V}_Y)$ are the orthographic projection of $\mathbf{R}$ and $\mathbf{V}$ on S respectively. $\mathtt{C}$ represents a real circle for $\tau = 0$.By observing the circle $\mathtt{C}$ into the image plane of the camera of optical center $\mathbf{V}$, a conic is obtained and more particularly, an ellipse if the specularity is entirely in the image plane.

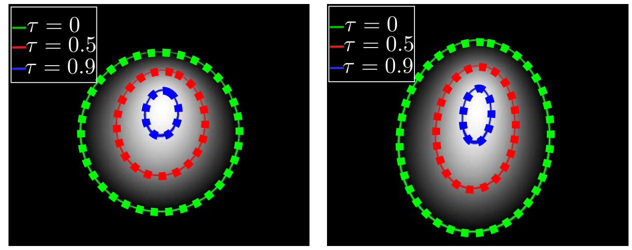

(a) (b)

Figure 3: Illustration of our hypothesis of conic shaped specularities. A specularity is generated from the specular term of Phong reflection model in (a) and from the specular term of Blinn-Phong reflection model in (b). In the latter, specularities are clearly elliptical whereas in Phong, they appeared as more circular shaped. By observing these shapes from the image plane of the camera, conics are obtained. If the specularity is entirely in the image plane these conics are ellipses. We show in these examples the different isocontours associated to a specific intensity $\tau = \{0, 0.5, 0.9\}$ (line contours in green, red and blue) along with the fitted conics (in dotted contours in green, red and blue). Our hypothesis of conic shaped specularity is clearly valid in these examples.

The inner isocontours. To study the inner isocontours which correspond to an arbitrary $\tau \in [0, 1]$, specular reflections could be approximated by conics using the Phong model as illustrated in figure 3(a). This approximation was also tested and validated with the Blinn-Phong [2] model as illustrated in figure 3(b). Initially this model was defined as an approximation of the Phong model, it is now often presented by the computer graphics community as more physically accurate than Phong's and commonly used in computer graphics. This model is physically better because it verifies the Helmholtz equation [13].

3.2 Empirical Validation on Simulated Data

To validate our conic approximation of specularities, we used the method of Fitzgibbon *et al.* [9] for ellipse fitting on different values of $\tau \in [0, 1]$ on the specular term alone and on the diffuse and specular terms combined. In an AR context, the diffuse and specular terms are correlated. For each value of τ, with a step of 0.05 between each value, we run 1000 scenarios of different light source and camera poses. The error is computed using the distance from Sturm *et al.* [35] between the fitted conic and the isocontours for each scenario. The specular and diffuse terms are generated using Phong [28] and Blinn-Phong [2] illumination models. The empirical validation of our conic approximation for different values of $\tau \in [0, 1]$ is illustrated in figure 4.

The error is computed as a ratio of the geometric distance with the diameter of the conic in pixels for $\tau = 0$. The results shows our approximation fits synthetic data with less than 1.5% of error confirming our conic representation to be reliable and accurate. We need to prove, for multiple viewpoints, the existence of a fixed quadric. We give an empirical validation in section 5.1.

For extended light sources such as fluorescent lamps, our conic shaped specularity approximation is still relevant. In computer graphics, an extended light source is generally represented as a set of point light sources *e.g* a line for fluorescent lamp. We have shown that for a single point light source, an associated conic can be found. Furthermore, we consider the outline of the specularity as the union of the associated conic for each point light source which is close to a conic. Thus, for an extended light source, a conic is still a good approximation for its associated specularity.

4 Model Estimation

We showed that the shape of specularities on a plane surface could be approximated by a conic. The main contribution of our method

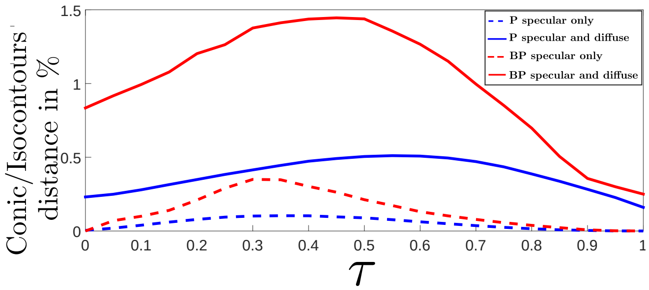

Figure 4: Empirical validation from simulated data. Our hypothesis of conic shaped specularity is tested on the Phong (P) and the Blinn-Phong (BP) illumination models for different values of intensity $\tau \in [0,1]$. This hypothesis is tested for the specular term alone and for the combination of the specular and diffuse terms. For each value of τ, with a step of 0.05 between each value, we run 1000 scenarios of different light source and camera poses. The error is computed using the distance from Sturm *et al.* [35] between the fitted conic and the isocontours for each scenario.

is to propose an empirical model for specularity prediction modeled by a quadric $\mathtt{Q}$ associated with its projections on the plane S for a given camera pose Π.

4.1 Overview

The pipeline of the proposed method is detailed as follows:

- Specularity detection in images
- Conic fitting on specularities on the planar surface
- Quadric reconstruction
- Perspective projection of the quadric to predict specularities in the image.

4.2 Quadric Reconstruction

We use the approach of Cross *et al.* [7] which reconstructs a dual quadric $\mathtt{Q}^*$ from several dual conics $\mathtt{C}^*$ in closed form by rewriting the relation:

$$\Pi \mathtt{Q}^* \Pi^\top = \mathtt{C}^*, \tag{9}$$

into a linear system. By vectorizing $\mathtt{Q}, \Pi$ and $\mathtt{C}$ as $\mathtt{Q}_v$, $\mathtt{B}$ and $\mathtt{C}_v$, we can build the equation (10) equivalent to using specular reflections as conics $\mathtt{C}$ and JOLIMAS as $\mathtt{Q}$ for n viewpoints with $n \geq 3$.

$$\mathtt{M}\mathtt{w} = 0 \Leftrightarrow$$

$$\begin{pmatrix} \mathtt{B}_1 & -\mathtt{C}^*_{1,v} & 0 & \dots & 0 \\ \mathtt{B}_2 & 0 & -\mathtt{C}^*_{2,v} & & 0 \\ \vdots & 0 & 0 & \ddots & \vdots \\ \mathtt{B}_n & 0 & 0 & \dots & -\mathtt{C}^*_{n,v} \end{pmatrix} \begin{pmatrix} \mathtt{Q}^*_v \\ \alpha_1 \\ \alpha_2 \\ \vdots \\ \alpha_n \end{pmatrix} = 0, \tag{10}$$

with $\mathtt{B}_i \in \mathbb{R}^{6\times 10}$. The solutions of system (10) are retrieved by a singular value decomposition (SVD) of $\mathtt{M}$. Note that α_i corresponds to a scale such that: $\alpha_i \mathtt{c}^*_{i,v} = \mathtt{B}_i \mathtt{Q}^*_{i,v}$ for the viewpoint i. The quadric reconstruction process is illustrated in figure 2. However, the system (10) is sensitive to the fitting errors of the input conics. To ensure the quality of the input conics used for the reconstruction, we compare two methods of epipolar correction of the input conics to ensure they respect the epipolar constraint for the quadric initialization process.

Conic epipolar correction. The epipolar correction of Cross *et al.* [7] consists of computing for each viewpoint the epipolar lines imposed from the other viewpoints (2 lines per viewpoint). Each conic is corrected by a non-linear refinement to fit the imposed epipolar lines. This correction presents some drawbacks. Indeed, the process is limited to 3 viewpoints (corresponding to 4 epipolar lines for each viewpoint). The epipolar lines are estimated from conics which are difficult to correct. The more the number of viewpoints, the less effective the epipolar correction. Additionally, recent approaches such as Reyes *et al.* [29] prove that the non-linear refinement process is not required.

Indeed, a conic is defined in an unique manner for 5 non-aligned points or 5 non-colinear lines in the dual space. For 3 viewpoints, each conic is constrained by two pairs of lines from other viewpoints which makes the dual conic estimation under-constrained. Reyes *et al.* [29] approach estimates a new epipolar line from the contours associated with the specularity in the image to compute the unique dual conic. This process is repeated for each contour point and viewpoint. The corrected conic fitting the 5 epipolar lines, such that the Conic-Point distance according to Sturm *et al.* [35], is minimal, replaces the previous conic allowing a quadric reconstruction where input conics respect the epipolar constraint. This method is iterative, efficient and reliable. However, in our context, our reconstruction cannot be limited to three viewpoints.

Non-linear refinement. To further improve the initialization, the quadric reconstruction of Reyes [29] also includes a non-linear refinement process minimizing the Conic-Point distance [35] between the quadric projections for each viewpoint and the associated contours. This method gives us a robust reconstruction of the quadric for 3+ viewpoints in real-time and usable for specularity prediction on unknown viewpoints. For these advantages, we used Reyes *et al.* [29] method for the epipolar correction, initialization and non-linear refinement.

5 Experimental Results

To evaluate the relevance and accuracy of our proposed parametric light source model, two experiments are conducted. We first analyze the performance of JOLIMAS for specularity prediction on synthetic data generated from the Phong and Blinn-Phong illumination models. Thereafter, this prediction ability is evaluated on four real sequences including different light source types such as bulb and fluorescent lamps.

5.1 Synthetic Data

We give the synthetic validation of our quadric approximation in JOLIMAS model. The simulated camera has a $50mm$ lens with a centered principal point. The images have $0.45\times 0.45mm$ pixels for a resolution of 1000×1000. Our scene is composed of a $20\times 20cm$ specular plane and we observe a moving specularity. We randomly select viewpoints and a light source above the plane. From the Phong and Blinn-Phong illumination models, for each $\tau \in [0,1]$, 100 quadric estimations are made using 100 viewpoints. We compute the geometric distance between the observed specularity in the image (which combines the diffuse and specular terms in real data) with the associated quadric projection to the viewpoint.

As shown in figure 5, our quadric approximation is efficient in producing accurate specularity predictions for $\tau \in [0,1]$ for both Blinn-Phong and Phong illumination models with respectively 0.3% and 0.5% of error on average according to the scene dimension. However, the refinement process does not play a big part on synthetic sequences where the conditions are ideal.

5.2 Real Data

We evaluated JOLIMAS on real sequences with three different light sources and five different materials. The quadric is reconstructed

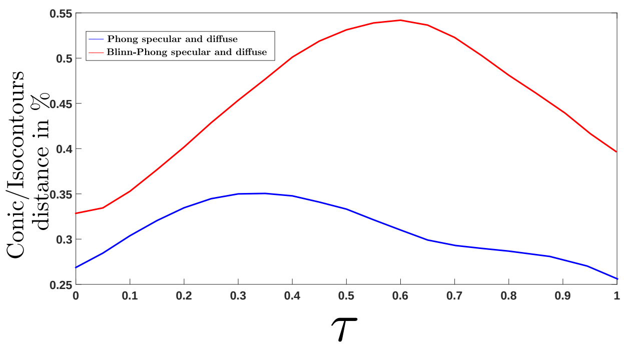

Figure 5: Validation of our model by measuring the prediction error on synthetic data. From 100 viewpoints, a fixed quadric is reconstructed and its projection is compared to specularity contours of each viewpoint using Sturm *et al.*'s distance [35]. For each value of $\tau = [0, 1]$ with a step of 0.05, 100 quadrics are estimated. We achieve an average error of 0.3% and 0.5% for the Blinn-Phong and Phong models respectively confirming the relevance and accuracy of our empirical model.

from conics fitted by the method of Fitzgibbon *et al.* [9]. The specularities are detected using the approach of Morgand *et al.* [25]. Camera poses are computed using a SLAM method [36]. The accuracy of our quadric model is evaluated on real data to quantify the prediction ability of our approach. We use the distance of Sturm *et al.* [35] to measure the Conic-Contour distance to the ground truth. To retrieve ground truth, we manually selected the specularities on the different sequences including light bulb and fluorescent lamps.

Our results are illustrated in the table 1, the figure 1 and figure 6.

2D distance (in pixels)	Initialization	Epipolar correction	Non-linear refinement
Light bulb 1 Steel table	110.3	82.2	62.8
Fluorescent lamp Kitchen counter	135.8	76.4	23.1
Fluorescent lamp Whiteboard	210.6	80.9	31.6
Light bulb 2 Electronic box	77.1	53.9	19.4
Light bulb 2 Plastic book	85.2	66.7	28.9

Table 1: Empirical validation of our model and its capacity to predict specular reflections in images for 5 real sequences. The average error of prediction per specularity is computed in pixels using Sturm *et al.*'s distance [35] between the predicted conic and detected contours specularity. This prediction is evaluated during three steps: the initialization alone, the epipolar correction and the non-linear refinement. We observed a significant decrease in error at each step.

In our context, the quadric initialization is not sufficient on its own to predict specularity accurately. Estimating reliable specularity contours is difficult in practice which highly impact the quadric reconstruction quality. Adding an epipolar correction to the outlines of the input conics provides better results. By combining the epipolar correction with the non-linear refinement, we achieve a maximum error value of 62.8 pixels. For real sequences, JOLIMAS is accurate and allows specularity prediction on new viewpoint for a variety of light sources.

6 Application to Dynamic Retexturing

A natural application of JOLIMAS is to reproduce a specularity on a planar surface while changing the texture. Indeed, from a physical model of light source, specularity prediction is difficult without computing numerous parameters of the light sources and materials.

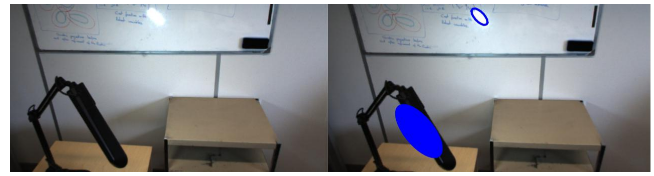

(a)

(b)

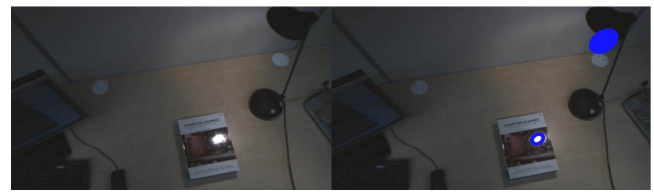

(c)

Figure 6: Specularity prediction on three real sequences a whiteboard illuminated by a fluorescent lamp (a), an electronic box illuminated from a light bulb (b) and a book illuminated by a light bulb (c). Our virtual model is projected on the different planes to fit the observed specularity (blue ellipses). We computed the symmetric from the planes (whiteboard, electronic box and book cover) to display the reconstructed quadric in JOLIMAS (blue ellipsoids), which happens to lie on the light sources.

One of the main interest of our model is to predict synthetic viewpoints (unknown viewpoints where the camera never went in the sequence). Our model is needed to predict specularities as opposed to simply detecting and fitting ellipses to the specularities. Indeed, the quality of specularity detection cannot be guaranteed for every viewpoint because of light conditions changes, specularity detector limitations, imperfections on the planar surface (roughness) and occluding objects in the scene. Thus, these issues could affect the conic fitting process and cause jittering and temporal incoherence in the retexturing rendering. For applications such as diminished reality, a stable prediction of specularities is needed to guarantee a convincing rendering.

We propose a simple approximation based on the specularity modeling by a 2D Gaussian function. Indeed, a specularity is described as a high intensity area. Starting from the center of this specularity, the intensity is progressively decreasing making the use of a Gaussian function appropriate. The Gaussian intensity function captures the following properties of the specularity: the smooth variation of the intensity and the ellipticity of the isocontours. In theory, the intensity distribution of a specularity may be more complex as the intensity at an isocontour depends on the angle between the incident light ray and the camera's optical axe: this angle is proportional to the isocontour's eccentricity.

Our retexturing method is divided in several steps. Firstly, from detected specularities in the sequence, a mean of the specularity color is computed to fit the lighting conditions. The appropriate Gaussian function is computed on the red, green and blue color channels to match the specularity detected in the sequences. To correctly draw our synthetic specularity on the texture associated to the plane, two homographies are computed: $\mathtt{H}_2$, the transforma-

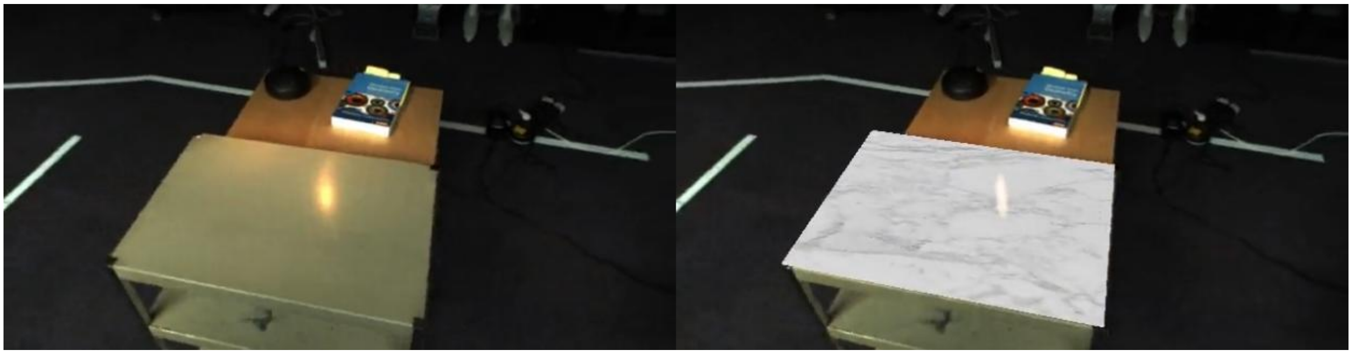

(a)

(b)

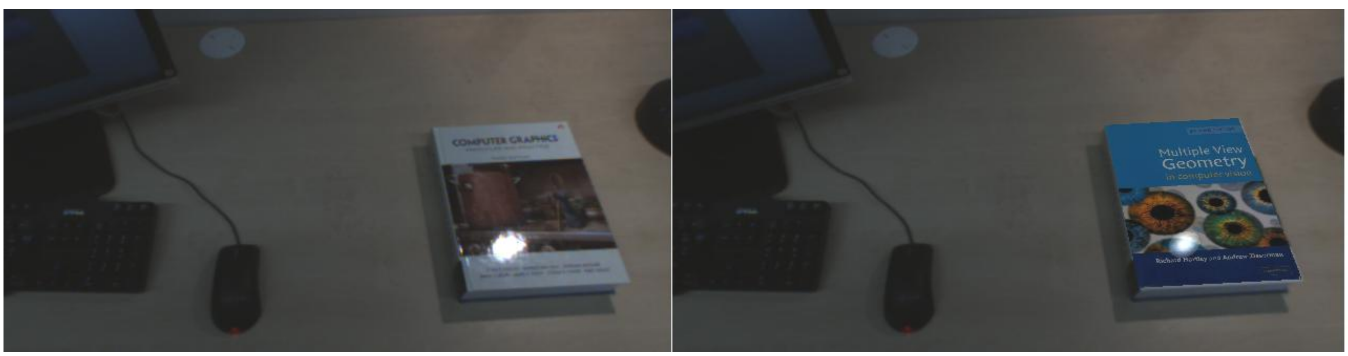

(c)

(d)

Figure 7: Retexturing method illustrated on the light bulb/steel table sequence (a) by using a marble texture, the fluorescent lamp/kitchen counter sequence (b) using a rock texturing, the light bulb/book sequence by switching the book cover (c) and the fluorescent lamp/whiteboard by changing the content on the whiteboard (d). To simulate the specularity, we used a Gaussian function and transformed it onto the plane surface using our specularity prediction to compute the transformation. The color of the specularity is computed from the specularities detected in the images used for the quadric reconstruction. Without considering the diffuse term on the texture, we can realistically change the texture of the planar surface using only the specular term predicted by JOLIMAS. The retexturing sequences can be found in the supplementary materials

tion from the texture to the planar surface and $\mathtt{H}_1$ transforming the unit circle into the predicted conic (the conic is first transformed by $\mathtt{H}_2^{-1}$). Our synthetic texture replaces the scene planar surface by merging the texture with our Gaussian texture using $\mathtt{H}_1$ and transforms the fusion onto the plane using $\mathtt{H}_2$. Three results of retexturing are shown in figure 7.

A better rendering quality could be obtained by modeling the diffuse term. However, the simplicity of our method provides good results with room for improvement with additional parameters (roughness or surface reflectance).

7 Discussion and Conclusion

We have presented a novel empirical and virtual model for specularity prediction called JOint LIght-MAterial Specularity (JOLIMAS). After observing the conic shape of a specularity on a planar surface, a detailed demonstration on the Phong and Blinn-Phong reflection models was conducted to confirm the relevance of this approximation. In projective geometry a quadric projection generates a conic. By proving the existence of a fixed virtual quadric whose projection is associated with a specularity on a viewpoint, we demonstrated a link between photometry (light and materials) and multiple view geometry (virtual quadric). This virtual quadric is reconstructed from conics fitted to specularities. This model was tested on synthetic and real sequences for various light source types such as light bulbs and fluorescent lamps. The specularity prediction ability of the model allows one to achieve dynamic retexturing by changing the plane texture and rendering a specularity predicted by JOLIMAS. The current state of JOLIMAS could be used to improve the realism of AR applications by rendering specularities and shadows on the augmentations. Moreover, this specularity prediction aspect could greatly improve camera localization algorithms. For computer graphics applications, the computation of the specular term could be quickly rendered using our predictions. We plan to generalize the approach for multiple light sources by tracking multiple specularities. We also plan to extend JOLIMAS to curved surfaces. This will require one to study how the surface's unflatness deforms the specularity's isocontours. In fact, the specularity shape seems related to the second derivative of the surface [10]. Thus, a link could be found between JOLIMAS and surface curvature.

8 Appendix : Analysis Specular Highlight Isocontours under the Phong and Blinn-Phong Models

Further explanations on the isocontours analysis are detailed here. We focused on the highlight's outline which corresponds to an intensity for $\tau = 0$.

8.1 Formalization and notations

Our scene is composed of a light source $\mathbf{L}$ with a viewpoint $\mathbf{V}$ and a planar surface S. We choose the world coordinate frame so that the scene's flat surface $S \subset \mathbb{R}^3$ is the $(\mathbf{XY})$ plane. In other words, $S = \{\mathbf{P} \in \mathbb{R}^3 | \mathbf{P}_Z = 0\}$. We can thus parameterize S by a point $\mathbf{p} \in \mathbb{R}^2$ and define $\mathbf{P} = \mathrm{stk}(\mathbf{p}, 0)$ with stk the stack operator for notation simplicity:

$$\mathrm{stk}(\mathbf{X}, \mathbf{Y}) = \begin{pmatrix} \mathbf{X} \\ \mathbf{Y} \end{pmatrix}$$

For Phong and Blinn-Phong illumination model, we use $\hat{\mathbf{R}}$ the normalized direction of a perfectly reflected ray of light $\hat{\mathbf{L}}$, $\hat{\mathbf{V}}$ the normalized direction pointing towards the viewer, n the glossiness of the surface, k_s, k_a and k_d the ratio of reflection of the specular, ambient and diffuse term of incoming light, $\hat{\mathbf{N}}$ the normal of the surface S and i_s, i_a and i_d the incoming intensity on the surface for the specular, ambient and diffuse term.

$\hat{\mathbf{V}}$ and $\hat{\mathbf{R}}$ are normalized vector such as: $\hat{\mathbf{V}}(\mathbf{p}) = \mu(\mathbf{V} - \mathbf{P})$ and $\hat{\mathbf{R}}(\mathbf{p}) = -\mu(\mathbf{R} - \mathbf{P})$ with μ the normalization operator:

$$\mu(\mathbf{A}) = \frac{\mathbf{A}}{||\mathbf{A}||}.$$

8.1.1 Phong Model

The Phong intensity function of a 3D surface point $\mathbf{p}$ is given by:

$$I(\mathbf{p}) = i_a k_a + i_d k_d (\hat{\mathbf{L}}(\mathbf{p}) \cdot \hat{\mathbf{N}}) + i_s k_s (\hat{\mathbf{R}}(\mathbf{p}) \cdot \hat{\mathbf{V}}(\mathbf{p}))^n. \tag{11}$$

At point $\mathbf{p}$, the specular component I_s is given by:

$$I_s(\mathbf{p}) = \max(0, (\hat{\mathbf{R}}(\mathbf{p}) \cdot \hat{\mathbf{V}}(\mathbf{p}))^n), \tag{12}$$

We want to analyze the isocontours of a specular highlight on the surface S for a viewpoint $\mathbf{V}$, a light source $\mathbf{L}$ and $\mathbf{R} = \mathrm{stk}(L_X, L_Y, -L_Z)$. We first expand Eq.(13) for a general τ and then solve it for $\tau = 1$ and $\tau = 0$.

$$I_s(\mathbf{p}) = \tau. \tag{13}$$

I_s is a scalar product between two normalized vectors, we have $-1 \leq I_s \leq 1$.

The specular term is proportional to:

$$I_s(\mathbf{p}) \propto \hat{\mathbf{R}}(\mathbf{p})^\top \hat{\mathbf{V}}(\mathbf{p}), \tag{14}$$

We expand (14) such as:

$$I_s(\mathbf{p}) \propto -\mu(\mathbf{R} - \mathbf{P})^\top \mu(\mathbf{V} - \mathbf{P}), \tag{15}$$

8.1.2 Blinn-Phong Model

The Blinn-Phong intensity function of a 3D surface point $\mathbf{p}$ is given by:

$$I(\mathbf{p}) = i_a k_a + i_d k_d (\hat{\mathbf{L}}(\mathbf{p}) \cdot \hat{\mathbf{N}}) + i_s k_s (\hat{\mathbf{N}} \cdot \hat{\mathbf{H}}(\mathbf{p}))^n, \tag{16}$$

with the half-way vector $\hat{\mathbf{H}}$:

$$\hat{\mathbf{H}} = \frac{\hat{\mathbf{L}}(\mathbf{p}) + \hat{\mathbf{V}}(\mathbf{p})}{||\hat{\mathbf{L}}(\mathbf{p}) + \hat{\mathbf{V}}(\mathbf{p})||}$$

The specular term is defined by:

$$I_s(\mathbf{p}) \propto \hat{\mathbf{N}}(\mathbf{p})^\top \frac{\hat{\mathbf{L}}(\mathbf{p}) + \hat{\mathbf{V}}(\mathbf{p})}{||\hat{\mathbf{L}}(\mathbf{p}) + \hat{\mathbf{V}}(\mathbf{p})||}, \tag{17}$$

We expand (17) such as:

$$I_s(\mathbf{p}) \propto \hat{\mathbf{N}}(\mathbf{p})^\top \frac{\mu(\mathbf{L} - \mathbf{P}) + \mu(\mathbf{V} - \mathbf{P})}{||\mu(\mathbf{L} - \mathbf{P}) + \mu(\mathbf{V} - \mathbf{P})||}, \tag{18}$$

In the same manner as Phong model, we want to analyze the isocontours of a specular highlight on the surface S for a viewpoint $\mathbf{V}$, a light source $\mathbf{L}$ and $\mathbf{R} = \mathrm{stk}(L_X, L_Y, -L_Z)$ from the Eq.(13).

8.2 Derivation for a General τ

8.2.1 Phong Model

By multiplying the equation by $||\mathbf{R} - \mathbf{P}||||\mathbf{V} - \mathbf{P}||$:

$$-(\mathbf{R} - \mathbf{P})^\top (\mathbf{V} - \mathbf{P}) = \tau ||\mathbf{R} - \mathbf{P}||||\mathbf{V} - \mathbf{P}||. \tag{19}$$

Squaring both sides and substracting the RHS, we obtain a bivariate quartic (in x and y):

$$((\mathbf{R} - \mathbf{P})^\top (\mathbf{V} - \mathbf{P}))^2 - \tau^2 ||\mathbf{R} - \mathbf{P}||^2 ||\mathbf{V} - \mathbf{P}||^2 = 0. \tag{20}$$

By expanding and collecting the monomials of same degrees, we have:

$(d^\circ 4)$ $(1-\tau^2)||\mathbf{P}||^4$

$(d^\circ 3)$ $2(\tau^2-1)(\mathbf{R}+\mathbf{V})^\top\mathbf{P}||\mathbf{P}||^2$

$(d^\circ 2)$ $\mathbf{P}^\top(\mathbf{R}\mathbf{R}^\top+2\tau(1-2\tau^2)\mathbf{R}\mathbf{V}^\top+$
$(2\mathbf{R}^\top\mathbf{V}-\tau^2||\mathbf{R}||^2-\tau^2||\mathbf{V}||^2)\mathtt{I})\mathbf{P}$

$(d^\circ 1)$ $2(-\mathbf{R}^\top\mathbf{V}\mathbf{R}^\top-\mathbf{R}^\top\mathbf{V}\mathbf{V}^\top+\tau^2||\mathbf{R}||^2\mathbf{V}^\top+\tau^2||\mathbf{V}||^2\mathbf{R}^\top)\mathbf{P}$

$(d^\circ 0)$ $(\mathbf{R}^\top\mathbf{V})^2-\tau^2||\mathbf{R}||^2||\mathbf{V}||^2$.

We observe the sum of degrees 3 and 4 factors as:

$$(1-\tau^2)||\mathbf{P}||^2\mathbf{P}^\top(\mathbf{P}-2\mathbf{R}-2\mathbf{V}).$$

It is thus small if τ is close to 1, meaning if we are close to the highlight's centre.

8.2.2 Blinn-Phong Model

The development of the specular term for a general τ in the Blinn-Phong model is not detailed here as it does not bring interesting information or special case.

Indeed, the analysis of the specular term for $\tau=1$ is not as straightforward as the Phong illumination model one. For simplicity purposes, we will only study the highlight's outer ring for $\tau=0$.

8.3 Analysis of the highlight's outer ring, $\tau=0$

8.3.1 Phong

In that case, we directly have (before squaring):

$$-(\mathbf{R}-\mathbf{P})^\top(\mathbf{V}-\mathbf{P})=0.$$

This is a quadric, whose intersection with S gives the sought conic. Expanding the above equation, we obtain:

$$||\mathbf{P}||^2-(\mathbf{R}+\mathbf{V})^\top\mathbf{P}+\mathbf{R}^\top\mathbf{V}=0,$$

which is a quadric whose point matrix is:

$$\mathtt{Q}=\begin{bmatrix}\mathtt{I}_3 & -\frac{1}{2}(\mathbf{R}+\mathbf{V})\\ -\frac{1}{2}(\mathbf{R}+\mathbf{V})^\top & \mathbf{R}^\top\mathbf{V}\end{bmatrix}.$$

We define the orthographic projection on S as:

$$\mathtt{A}=\begin{bmatrix}1&0&0\\0&1&0\\0&0&0\\0&0&1\end{bmatrix}. \tag{21}$$

The highlight's outer ring is thus given by the conic:

$$\mathtt{C}=\mathtt{A}^\top\mathtt{Q}\mathtt{A}=\begin{bmatrix}\mathtt{I}_2 & -\frac{1}{2}(\bar{\mathbf{R}}+\bar{\mathbf{V}})\\ -\frac{1}{2}(\bar{\mathbf{R}}+\bar{\mathbf{V}})^\top & \mathbf{R}^\top\mathbf{V}\end{bmatrix},$$

with $\bar{\mathbf{R}}\stackrel{\text{def}}{=}\text{stk}(\mathbf{R}_X,\mathbf{R}_Y)$ and $\bar{\mathbf{V}}\stackrel{\text{def}}{=}\text{stk}(\mathbf{V}_X,\mathbf{V}_Y)$ the orthographic projection of $\mathbf{R}$ and $\mathbf{V}$ on S respectively. $\mathtt{C}$ represents a real circle if $\det(\mathtt{C})<0$ and an imaginary circle otherwise.

8.3.2 Blinn-Phong Model

We solve the equation for $\tau=0$:

$$\hat{\mathbf{N}}(\mathbf{p})^\top\frac{\mu(\mathbf{L}-\mathbf{P})+\mu(\mathbf{V}-\mathbf{P})}{||\mu(\mathbf{L}-\mathbf{P})+\mu(\mathbf{V}-\mathbf{P})||}=0.$$

By expanding and collecting the monomials of same degrees, we have:

$(d^\circ 4)$ $\mathbf{P}_Z||\mathbf{P}||^2$

$(d^\circ 3)$ $-2(\mathbf{L}_Z\mathbf{P}_Z||\mathbf{P}||^2-\mathbf{V}_Z\mathbf{P}_Z||\mathbf{P}||^2-\mathbf{P}^\top\mathbf{L}\mathbf{P}_Z^2+\mathbf{P}^\top\mathbf{V}\mathbf{P}_Z^2)$

$(d^\circ 2)$ $4(\mathbf{L}_Z\mathbf{P}_Z\mathbf{P}^\top\mathbf{V}-\mathbf{V}_Z\mathbf{P}_Z\mathbf{P}^\top\mathbf{L})+$
$\mathbf{P}_Z^2(||\mathbf{V}||^2-||\mathbf{L}||^2)+(\mathbf{L}_Z^2-\mathbf{V}_Z^2)||\mathbf{P}||^2$

$(d^\circ 1)$ $2(\mathbf{V}_Z\mathbf{P}_Z||\mathbf{L}||^2-\mathbf{L}_Z\mathbf{P}_Z||\mathbf{V}||^2+\mathbf{V}_Z^2\mathbf{P}^\top\mathbf{L}-\mathbf{L}_Z^2\mathbf{P}^\top\mathbf{V})$

$(d^\circ 0)$ $\mathbf{L}_Z^2||\mathbf{V}||^2-\mathbf{V}_Z^2||\mathbf{L}||^2$.

We note that, $\mathbf{P}=\text{stk}(\mathbf{p},0)$ with $\mathbf{p}=\text{stk}(\mathbf{p}_X,\mathbf{p}_Y)$. With $\mathbf{P}_Z=0$, the degrees 4 and 3 vanish:

$(d^\circ 2)$ $(\mathbf{L}_Z^2-\mathbf{V}_Z^2)||\mathbf{P}||^2$

$(d^\circ 1)$ $2(\mathbf{V}_Z^2\mathbf{L}^\top-\mathbf{L}_Z^2\mathbf{V}^\top)\mathbf{P}$

$(d^\circ 0)$ $\mathbf{L}_Z^2||\mathbf{V}||^2-\mathbf{V}_Z^2||\mathbf{L}||^2$.

The monomials can be factored in the following form:

$$\tilde{\mathbf{P}}^\top\mathtt{Q}\tilde{\mathbf{P}}=0, \tag{22}$$

where $\tilde{\mathbf{P}}\stackrel{\text{def}}{=}\text{stk}(\mathbf{P},1)$ are the homogeneous coordinates of $\mathbf{P}$. Matrix $\mathtt{Q}\in\mathbb{R}^{4\times4}$ is symmetric and defined by:

$$\mathtt{Q}=\begin{bmatrix}\mathbf{L}_Z^2-\mathbf{V}_Z^2 & (\mathbf{V}_Z^2\mathbf{L}-\mathbf{L}_Z^2\mathbf{V})^\top\\ \mathbf{V}_Z^2\mathbf{L}-\mathbf{L}_Z^2\mathbf{V} & \mathbf{L}_Z^2||\mathbf{V}||^2-\mathbf{V}_Z^2||\mathbf{L}||^2.\end{bmatrix} \tag{23}$$

We define the orthographic projection on S as:

$$\mathtt{A}=\begin{bmatrix}1&0&0\\0&1&0\\0&0&0\\0&0&1\end{bmatrix}.$$

The highlight's outer ring is thus given by the conic:

$$\mathtt{C}=\mathtt{A}^\top\mathtt{Q}\mathtt{A}=\begin{bmatrix}\mathbf{L}_Z^2-\mathbf{V}_Z^2 & (\mathbf{V}_Z^2\bar{\mathbf{L}}-\mathbf{L}_Z^2\bar{\mathbf{V}})^\top\\ \mathbf{V}_Z^2\bar{\mathbf{L}}-\mathbf{L}_Z^2\bar{\mathbf{V}} & \mathbf{L}_Z^2||\mathbf{V}||^2-\mathbf{V}_Z^2||\mathbf{L}||^2\end{bmatrix},$$

with $\bar{\mathbf{V}}\stackrel{\text{def}}{=}\text{stk}(\mathbf{V}_X,\mathbf{V}_Y)$ and $\bar{\mathbf{L}}\stackrel{\text{def}}{=}\text{stk}(\mathbf{L}_X,\mathbf{L}_Y)$ are the orthographic projection of $\mathbf{V}$ and $\mathbf{L}$ on S respectively. $\mathtt{C}$ represents a real circle.

8.4 Special case, analysis for $\tau=1$ for Phong Model

The study of $\tau=1$ concerns the points on the surface $\mathbf{S}$ of maximum intensity. For Phong model, this study is interesting because for $\tau=1$, the terms of degrees 3 and 4 vanish. The remaining terms are:

$(d^\circ 2)$ $\mathbf{P}^\top[\mathbf{R}-\mathbf{V}]_\times^2\mathbf{P}$

$(d^\circ 1)$ $2\mathbf{P}^\top[\mathbf{V}\times\mathbf{R}]_\times(\mathbf{V}-\mathbf{R})$

$(d^\circ 0)$ $(\mathbf{R}^\top\mathbf{V})^2-\tau^2||\mathbf{R}||^2||\mathbf{V}||^2$.

They can be factored in the following form:

$$\tilde{\mathbf{P}}^\top\mathtt{Q}\tilde{\mathbf{P}}=0, \tag{24}$$

where $\tilde{\mathbf{P}}\stackrel{\text{def}}{=}\text{stk}(\mathbf{P},1)$ are the homogeneous coordinates of $\mathbf{P}$. Matrix $\mathtt{Q}\in\mathbb{R}^{4\times4}$ is symmetric and defined by:

$$\mathtt{Q}=\begin{bmatrix}[\mathbf{R}-\mathbf{V}]_\times^2 & [\mathbf{V}\times\mathbf{R}]_\times(\mathbf{V}-\mathbf{R})\\ ([\mathbf{V}\times\mathbf{R}]_\times(\mathbf{V}-\mathbf{R}))^\top & (\mathbf{R}^\top\mathbf{V})^2-||\mathbf{R}||^2||\mathbf{V}||^2\end{bmatrix}$$

It thus represent a quadric, and $\hat{\mathbf{P}}$ lies at the intersection of this quadric with S. The leading (3×3) block of $\mathtt{Q}$ is $[\mathbf{R}-\mathbf{V}]_\times^2$ and thus has rank 2. Therefore, $\mathrm{rank}(\mathtt{Q}) \geq 2$. We show below that $\mathbf{Q}\tilde{\mathbf{R}} = \mathbf{Q}\tilde{\mathbf{V}} = 0$. This means $\mathrm{rank}(\mathtt{Q}) \leq 2$ and thus that $\mathrm{rank}(\mathtt{Q}) = 2$. This also means that $\mathtt{Q}$ is semi-definite, either non-positive or non-negative. The way we constructed the polynomial, starting from a fraction $I_s = \frac{a}{b} = \tau = 1$, with $a \leq b$ imply $a - b \leq 0$ and thus that $\mathtt{Q}$ is a point quadric representing the line containing $\mathbf{R}$ and $\mathbf{V}$. Its intersection with S then yields the expected solution for $\hat{\mathbf{P}}$.

Showing $\tilde{\mathbf{R}} \in \mathtt{Q}^\perp$. We have the leading part as:

$$[\mathbf{R}-\mathbf{V}]_\times^2 + [\mathbf{V}\times\mathbf{R}]_\times(\mathbf{V}-\mathbf{R}).$$

The first term is expanded as:

$$\begin{aligned}&[\mathbf{R}-\mathbf{V}]_\times[\mathbf{R}-\mathbf{V}]_\times\mathbf{R}\\ &= [\mathbf{R}-\mathbf{V}]_\times[\mathbf{V}]_\times\mathbf{R}\\ &= [\mathbf{V}]_\times^2\mathbf{R} - [\mathbf{R}]_\times[\mathbf{V}]_\times\mathbf{R}\\ &= \mathbf{V}\times(\mathbf{V}\times\mathbf{R}) - \mathbf{R}\times(\mathbf{V}\times\mathbf{R}).\end{aligned}$$

The second term is expanded as:

$$(\mathbf{V}\times\mathbf{R})\times\mathbf{R} - (\mathbf{V}\times\mathbf{R})\times\mathbf{R} = -\mathbf{V}\times(\mathbf{V}\times\mathbf{R}) + \mathbf{R}\times(\mathbf{V}\times\mathbf{R}),$$

which sum to zero. The last element is:

$$(\mathbf{R}-\mathbf{V})^\top[\mathbf{V}\times\mathbf{R}]_\times\mathbf{R} + (\mathbf{R}^\top\mathbf{V})^2 - ||\mathbf{R}||^2||\mathbf{V}||^2.$$

The first term is expanded as:

$$(\mathbf{R}-\mathbf{V})^\top(\mathbf{R}\times(\mathbf{R}\times\mathbf{V})) = -\mathbf{V}^\top(\mathbf{R}\times(\mathbf{R}\times\mathbf{V})) = -\mathbf{V}^\top[\mathbf{R}]_\times^2\mathbf{V}.$$

We saw that the second and third terms (the degree 0 coefficients of the polynomial) are also equal to $\mathbf{V}^\top[\mathbf{R}]_\times^2\mathbf{V}$, which concludes.

8.5 Conclusion for a general τ

For both models, the analysis of I_s shows a circle for $\tau = 0$. From the viewpoint of a camera pointing to the plane with $\mathbf{V}$ its optical center, we obtain an conic for $\tau = 0$ and an ellipse if the circle is entirely seen in the image plane.d We empirically studied the specularity shape on both models for a general τ in the submission.

Note that for Phong model, the analysis of I_s shows a point on S for $\tau = 1$ which corresponds to the brightest point.

References

[1] A. Blake. Does the brain know the physics of specular reflection? *Nature*, 343(6254):165–168, 1990.

[2] J. F. Blinn. Models of light reflection for computer synthesized pictures. In *ACM SIGGRAPH Computer Graphics*, SIGGRAPH, 1977.

[3] B. J. Boom, S. Orts-Escolano, X. X. Ning, S. McDonagh, P. Sandilands, and R. B. Fisher. Point light source estimation based on scenes recorded by a rgb-d camera. In *British Machine Vision Conference*, BMVC, 2013.

[4] P.-E. Buteau and H. Saito. Retrieving lights positions using plane segmentation with diffuse illumination reinforced with specular component. In *International Symposium on Mixed and Augmented Reality*, ISMAR, 2015.

[5] J. Y. Chang, R. Raskar, and A. Agrawal. 3d pose estimation and segmentation using specular cues. In *Computer Vision and Pattern Recognition*, CVPR, 2009.

[6] R. L. Cook and K. E. Torrance. A reflectance model for computer graphics. *Transactions on Graphics*, 1(1):7–24, 1982.

[7] G. Cross and A. Zisserman. Quadric reconstruction from dual-space geometry. In *International Conference on Computer Vision*, ICCV, 1998.

[8] M. Csongei, L. Hoang, and C. Sandor. Interactive near-field illumination for photorealistic augmented reality on mobile devices. In *Virtual Reality*, VR, 2014.

[9] A. W. Fitzgibbon, R. B. Fisher, et al. A buyer's guide to conic fitting. *DAI Research paper*, 1996.

[10] R. W. Fleming, A. Torralba, and E. H. Adelson. Specular reflections and the perception of shape. *Journal of Vision*, 4(9):10, 2004.

[11] L. Gruber, T. Langlotz, P. Sen, T. Hoherer, and D. Schmalstieg. Efficient and robust radiance transfer for probeless photorealistic augmented reality. In *Virtual Reality*, VR, 2014.

[12] T. Hachisuka, S. Ogaki, and H. W. Jensen. Progressive photon mapping. In *ACM Transactions on Graphics (TOG)*, volume 27, page 130, 2008.

[13] E. Haines and T. Akenine-Moller. Real-time rendering. 2002.

[14] R. I. Hartley and A. Zisserman. *Multiple View Geometry in Computer Vision*. Cambridge University Press, ISBN: 0521540518, second edition, 2004.

[15] G. B. Hughes and M. Chraibi. Calculating ellipse overlap areas. *Computing and Visualization in Science*, 15(5):291–301, 2012.

[16] J. Jachnik, R. A. Newcombe, and A. J. Davison. Real-time surface light-field capture for augmentation of planar specular. In *International Symposium on Mixed and Augmented Reality*, ISMAR, 2012.

[17] W. Jarosz, M. Zwicker, and H. W. Jensen. The beam radiance estimate for volumetric photon mapping. SIGGRAPH, 2008.

[18] M. Kanbara and N. Yokoya. Real-time estimation of light source environment for photorealistic augmented reality. In *International Conference on Pattern Recognition*, ICPR, 2004.

[19] S. B. Knorr and D. Kurz. Real-time illumination estimation from faces for coherent rendering. In *International Symposium on Mixed and Augmented Reality*, ISMAR, 2014.

[20] P. Lagger and P. Fua. Using specularities to recover multiple light sources in the presence of texture. In *International Conference on Pattern Recognition*, ICPR, 2006.

[21] P. Lagger, M. Salzmann, V. Lepetit, and P. Fua. 3d pose refinement from reflections. In *Computer Vision and Pattern Recognition*, CVPR, 2008.

[22] C. Lindsay and E. Agu. Automatic multi-light white balance using illumination gradients and color space projection. In *International Symposium on Visual Computing*, ISVC, 2014.

[23] M. Meilland, C. Barat, and A. Comport. 3d high dynamic range dense visual slam and its application to real-time object re-lighting. In *International Symposium on Mixed and Augmented Reality*, ISMAR, 2013.

[24] M. Meilland, A. Comport, P. Rives, and I. S. A. Méditerranée. Real-time dense visual tracking under large lighting variations. In *British Machine Vision Conference*, BMVC, 2011.

[25] A. Morgand and M. Tamaazousti. Generic and real-time detection of specular reflections in images. In *8th International Joint Conference on Computer Vision, Imaging and Computer Graphics Theory and Applications*, VISAPP, 2014.

[26] A. Netz and M. Osadchy. Recognition using specular highlights. In *Computer Vision and Pattern Recognition*, CVPR, 2013.

[27] A. Netz and M. Osadchy. Recognition using specular highlights. *Pattern Analysis and Machine Intelligence*, 35(3):639–652, 2013.

[28] B. T. Phong. Illumination for computer generated pictures. *Communications of the ACM*, 18(6):311–317, 1975.

[29] L. Reyes and E. Bayro-Corrochano. The projective reconstruction of points, lines, quadrics, plane conics and degenerate quadrics using uncalibrated cameras. *Image and Vision Computing*, 23(8):693–706, 2005.

[30] K. Rohmer, W. Buschel, R. Dachselt, and T. Grosch. Interactive near-field illumination for photorealistic augmented reality on mobile devices. In *International Symposium on Mixed and Augmented Reality*, ISMAR, 2014.

[31] I. Sato, Y. Sato, and K. Ikeuchi. Acquiring a radiance distribution to superimpose virtual objects onto a real scene. *Visualization and Computer Graphics, IEEE Transactions on*, 5(1):1–12, 1999.

[32] S. Savarese, L. Fei-Fei, and P. Perona. What do reflections tell us about the shape of a mirror? In *Proceedings of the 1st Symposium on Applied perception in graphics and visualization*, pages 115–118. ACM, 2004.

[33] N. Shroff, Y. Taguchi, O. Tuzel, A. Veeraraghavan, S. Ramalingam, and H. Okuda. Finding a needle in a specular haystack. In *International Conference on Robotics and Automation*, ICRA, 2011.

[34] G. Silveira and E. Malis. Real-time visual tracking under arbitrary illumination changes. In *Computer Vision and Pattern Recognition*, CVPR, 2007.

[35] P. Sturm and P. Gargallo. Conic fitting using the geometric distance. In *Asian Conference on Computer Vision*, ACCV. 2007.

[36] M. Tamaazousti, V. Gay-Bellile, S. Naudet Collette, S. Bourgeois, and M. Dhome. Nonlinear refinement of structure from motion reconstruction by taking advantage of a partial knowledge of the environment. In *Computer Vision and Pattern Recognition*, CVPR, 2011.

[37] G. J. Ward. The radiance lighting simulation and rendering system. In *Special Interest Group on Computer Graphics and Interactive Techniques*, SIGGRAPH, 1994.

[38] K.-Y. K. Wong, D. Schnieders, and S. Li. Recovering light directions and camera poses from a single sphere. In *European Conference on Computer Vision*, ECCV. 2008.